Pergamon

0360-5442(95)00125-5

Energy Vol. 21, No. 3, pp. 205–222, 1996

0360-5442/96 $15.00 + 0.00

THERMODYNAMIC ANALYSIS OF THE CO-PRODUCTION OF ZINC AND SYNTHESIS GAS USING SOLAR PROCESS HEAT

A. STEINFELD

Laboratory for Energy and Process Technology
Paul Scherrer Institute, CH-5232 Villigen-PSI, Switzerland

C. LARSON, R. PALUMBO, and M. FOLEY III

Mechanical Engineering Department
Valparaiso University, Valparaiso, IN 46383, U.S.A.

(Received 25 Sept. 1995)

Abstract — We present a solar thermochemical process that combines the reduction of zinc oxide with the reforming of natural gas (NG) for the co-production of zinc and syngas. The overall reaction may be represented by $ZnO+CH_4 = Zn+2H_2+CO$. The maximum possible overall efficiency is assessed for an ideal, closed cyclic system that recycles all materials and also for a more technically-feasible open system that allows for material flow into and out of the system. Assuming that the equilibrium chemical composition is obtained in a blackbody solar reactor operated at 1250 K, 1 atm, and with a solar power-flux concentration of 2000, closed-cycle efficiencies vary between 40 and 65%, depending on recovery of the product sensible heat. Under the same baseline conditions, open-cycle efficiencies vary between 36 and 50%, depending on whether a Zn/O_2 or an H_2/O_2 fuel cell is employed. Compared to the HHV of methane for generating electricity, the proposed solar open-cycle process releases half as much CO_2 to the atmosphere. The process modelling described in this paper establishes a base for evaluating and comparing different solar thermochemical processes.

1. INTRODUCTION

Solar thermochemical processes are endothermic processes that make use of concentrated solar energy as the source of high-temperature process heat. An example of such processes is the reduction of metal oxides. The products are metals that are usable as solid fuels for generating either heat via combustion, electricity via fuel cells, or hydrogen via water-splitting reactions; the hydrogen may be further processed for heat and electricity generation. The chemical products from these power-generating processes are metal oxides which, in turn, are recycled to the solar reactor. These cycles place solar energy in motion: solar radiation falling on uninhabited deserts can be transformed to chemical energy for transportation to industrialized regions. Metal oxide reduction processes that have been experimentally studied in solar furnaces include the production of Fe, Al, Mg, Zn, TiC, SiC, CaC_2, TiN, Si_3N_4, and AlN by carbothermic reduction of their oxides in Ar or N_2 atmospheres,[1-5] high-temperature electrolysis of ZnO and MgO,[6,7] and the thermal decomposition of Fe_3O_4, Mn_3O_4, and other oxides.[8-11]

Using NG as a reducing agent combines the reduction of metal oxides with the reforming of methane for the co-production of metals and synthesis gas (syngas). The overall reaction may be represented by

$$M_xO_y + yCH_4 = xM + y(2H_2 + CO) \ , \qquad (1)$$

where M denotes a metal and M_xO_y denotes the corresponding metal oxide. The chemical equilibrium composition of the system $M_xO_y+yCH_4$ has been studied for various metal oxides of industrial interest, viz., Fe_3O_4, ZnO, Al_2O_3, MgO, SiO_2, and TiO_2.[12] The CH_4-reduction of ZnO has been proposed using process heat from high-temperature gas-cooled nuclear reactors.[13] Also, the kinetics of the reduction of Fe_2O_3, Fe_3O_4 and ZnO with CH_4 have been investigated in laboratory electric furnaces.[14-19] Finally, the Fe_3O_4-CH_4 and ZnO-CH_4 systems produced the corresponding metal and syngas at 1300 K using a small-scale, fluidized-bed reactor at PSI's solar furnace.[20-23] These prior experiences indicate that a solar process technology for the proposed reactions can be developed.

Among the metal oxides studied, ZnO appears to be especially well suited for the combined solar M_xO_y-reduction/CH_4-reforming process. For ZnO, Eq. (1) becomes

$$ZnO + CH_4 = Zn + 2H_2 + CO \quad . \tag{2}$$

$\Delta G°$ of Eq. (2) equals zero at 1105 K. Thus, thermodynamics predict that at temperatures above 1105 K, the reaction proceeds to the right producing each of the gases at 1 bar when thermal energy equal to ΔH of the reaction (about 400 kJ per mole of Zn produced) is supplied. As will be shown in the following analysis, the chemical equilibrium composition of the system ZnO+CH_4 at 1250 K and 1 atm is essentially a gas-phase mixture containing Zn (vapor) and a 2:1 mixture of H_2 and CO. The reaction reaches completion at relatively moderate temperatures compared to those required to reduce other metal oxides such as MgO and Al_2O_3. Furthermore, no carbides or other undesirable products are formed, as opposed to the stable carbides and oxycarbides that result from the reduction of SiO_2, TiO_2 and Al_2O_3.[5,12] In contrast to the Fe_3O_4-CH_4 system, no significant carbon deposition has been observed experimentally.[19,21] An additional intriguing characteristic of the system ZnO-CH_4 is that Zn is recovered in the vapor phase, which allows for a natural phase separation from its solid oxide.

In this paper, we present a second-law analysis that assesses the maximum possible efficiency of a solar thermochemical process converting ZnO and CH_4 into Zn and syngas. We consider a closed cyclic system and one that is open but quasi-cyclic. In the closed system, only energy crosses the system boundaries, whereas energy and mass cross the boundaries of the open system. The two systems enable us to compare possible solar process schemes for extracting power from the chemical products. For each system, we investigate the influence of the operating temperature and pressure on its thermal performance and on the quality of its products. Furthermore, we identify the major sources of irreversibility and link them to the degradation in overall efficiency.

2. SOLAR ABSORPTION EFFICIENCY

The capability of a solar receiver to absorb the incoming solar power is a function of its geometrical configuration, its heat-transfer characteristics and, above all, its operating temperature. Previous studies of receivers and reactors for highly concentrated solar systems have featured the use of cavity-type configurations.[24] A cavity-receiver is a well insulated enclosure with a small opening, the *aperture*, that intercepts incoming solar radiation. Because of multiple reflections among the inner walls, the fraction of the incoming energy absorbed by the cavity exceeds the surface absorptance of the inner walls. However, at temperatures above about 1000 K, the net power absorbed is diminished mostly by radiative losses through the aperture. The solar energy absorption efficiency of a cavity-receiver $\eta_{absorption}$ accounts for this phenomenon. It is defined as the net rate at which energy is being absorbed divided by the solar power coming from the concentrator. For a perfectly insulated cavity receiver (no convection or conduction heat losses), it is given by[25]

$$\eta_{absorption} = \left(\alpha_{eff} Q_{aperture} - \varepsilon_{eff} A_{aperture} \sigma T_{cav}^4\right) \Big/ Q_{solar} \quad , \tag{3}$$

where Q_{solar} is the total power coming from the concentrator, $Q_{aperture}$ the amount intercepted by the aperture of area $A_{aperture}$, α_{eff} and ε_{eff} are the effective absorptance and emittance of the cavity-receiver, respectively,† T_{cav} is the nominal cavity temperature, and σ is the Stefan-Boltzmann constant. The first term in the numerator denotes the total power absorbed and the second term denotes the re-radiation losses, viz.,

$$Q_{absorbed} = \alpha_{eff} Q_{aperture} \quad , \tag{4}$$

$$Q_{rerad} = \varepsilon_{eff} A_{aperture} \sigma T_{cav}^4 \quad . \tag{5}$$

† α_{eff} is defined as the fraction of energy entering through the aperture that is absorbed by the cavity walls. For a gray-walled cavity and diffusely incident radiation, α_{eff} is equal to the apparent absorptance, defined as the fraction of energy flux emitted by a blackbody surface stretched across the aperture that is absorbed by the cavity walls.[26]

Their difference yields the net power absorbed by the reactor

$$Q_{reactor,\,net} = Q_{absorbed} - Q_{rerad} \quad . \tag{6}$$

Q_{solar}, the incoming solar power, is determined by the normal beam insolation I and by the collector area A_{coll} normal to the sun's rays, i.e.

$$Q_{solar} = \eta_{coll} A_{coll} I \quad , \tag{7}$$

where η_{coll} accounts for the optical imperfections of the collection system (e.g., reflectivity, specularity, tracking imperfections). Because of spilled radiation, $Q_{aperture} \leq Q_{solar}$. The capability of the collection system to concentrate solar energy and minimize spillage is often expressed in terms of its mean flux concentration ratio $\tilde{C}$ over an aperture, normalized to the incident normal beam insolation as follows:

$$\tilde{C} = Q_{aperture} / I\, A_{aperture} \quad . \tag{8}$$

The flux concentration ratio can be increased by increasing the optical precision of our primary collection system or by using non-imaging secondary reflectors (e.g., a compound parabolic concentrator, often referred to[27] as CPC). Higher $\tilde{C}$ would allow a smaller aperture to intercept the same amount of energy, thus reducing Q_{rerad}. Although larger apertures intercept more sunlight reflected from imperfect and imperfectly matched heliostats and concentrators, they also re-radiate more energy. Therefore, the optimum aperture size results from a compromise between maximizing radiation capture and minimizing re-radiation losses. Such optimization strongly depends on the incident solar flux distribution at the aperture plane of the receiver. The case of a Gaussian distribution has been examined analytically.[25] For simplification, we assume an aperture size that captures all incoming power so that $Q_{aperture} = Q_{solar}$. With this assumption, Eqs. (3) and (8) are combined to yield:

$$\tilde{C} = \eta_{coll}\left(A_{coll} / A_{aperture}\right) \tag{9}$$

and

$$\eta_{absorption} = \alpha_{eff} - \varepsilon_{eff}\left(\sigma T_{cav}^4 / I\tilde{C}\right) \quad . \tag{10}$$

With real receivers the absorption efficiency is even lower than stated in Eq. (10), because the inner walls of the cavity are usually at the highest temperature of the system and conductive losses to the outer shell become significant. These heat losses can be lowered to acceptable levels by lining the receiver with proper insulation.

Recently, novel receiver concepts have been proposed as alternatives to the conventional insulated cavity-receiver. For example, volumetric reactors use directly irradiated gas-particle suspensions to serve as radiant absorbers, heat-transfer medium, and chemical reactants.[28,29] Also, receivers having specular reflective inner walls prevent infrared radiation emitted by hot reactors and reactants from escaping the receiver or from being absorbed at the walls; instead, radiation is re-directed back to the reaction site.[30] These innovative configurations offer intriguing advantages in some specific applications. However, they are also subject to radiation losses from hot surfaces/gases towards the opening through which solar radiation enters. If the aperture is sufficiently small compared to the cavity enclosure, the fraction of intercepted radiation escaping becomes negligible regardless of the absorptivity of the inner walls. Thus, a perfectly insulated isothermal cavity, with a non-selective window, approaches a blackbody. In the analysis that follows, we assume $\alpha_{eff} = \varepsilon_{eff} = 1$.

3. OVERALL SYSTEM EFFICIENCY

The absorbed concentrated solar radiation drives the endothermic chemical reaction given by Eq. (2). The overall system efficiency of such thermochemical conversion is defined as the ratio of the Gibbs free energy change of the reaction to the solar power input, i.e.,

$$\eta_{overall} = -\Delta G|_{\text{Reactants}\rightarrow\text{Products}} / Q_{\text{solar}} \quad . \tag{11}$$

The conversion of solar process heat to the ΔG of the reaction is limited by both the solar absorption efficiency and the Carnot efficiency. The overall ideal system efficiency is then represented by

$$\eta_{overall,\,ideal} = \eta_{absorption} \times \eta_{Carnot} = \left[\left(Q_{absorbed} - Q_{rerad}\right)/Q_{solar}\right] \times \left[1 - \left(T_L/T_H\right)\right] \quad , \tag{12}$$

where T_H and T_L are the upper and lower operating temperatures of the equivalent Carnot heat engine. Therefore, from a thermodynamic standpoint, one should try to operate thermochemical processes at the highest upper temperature possible; however, from a heat-transfer perspective, the higher the temperature, the higher the re-radiation losses. The highest temperature an ideal solar cavity-receiver is capable of achieving is calculated by setting Eq. (12) equal to zero, which yields

$$T_{max} = \left(I\tilde{C}/\sigma\right)^{0.25} \quad . \tag{13}$$

For $\tilde{C}$=2000 and a typical normal beam solar insolation of 900 W/m^2, the highest attainable temperature is 2374 K. At this temperature, $\eta_{overall,\,ideal} = 0$ because energy is being re-radiated as fast as it is received. An energy-efficient process must run at temperatures that are substantially below T_{max}. If T_H is taken to be equal to T_{cav}, there is an optimum temperature for maximum efficiency obtained by setting

$$\partial \eta_{overall,\,ideal}/\partial T = 0 \quad . \tag{14}$$

Assuming uniform power-flux distribution, this relation yields the following implicit equation for T_{opt}:

$$T_{opt}^5 - (0.75T_L)T_{opt}^4 - \left(\alpha_{eff} T_L I\tilde{C}/4\varepsilon_{eff}\sigma\right) = 0 \quad . \tag{15}$$

Equation (15) was solved numerically.[31] For uniform power-flux distributions (which are likely to be obtained when non-imaging secondary concentrators are used in tandem with paraboloidal reflectors), T_{opt} varies between 1100 and 1800K for concentrations between 1000 and 13000. For example, when $\tilde{C}$=2000, I=900 W/m^2, and T_L=298 K, $\eta_{overall,\,ideal}$ is a maximum at about 1250 K. For a gaussian incident power-flux distribution having peak concentrations between 1000 and 12000, T_{opt} varies from 800 to 1300 K. In practice, when considering convection and conduction losses in addition to radiation losses, the efficiency will peak at a somewhat lower temperature. Nevertheless, the chemical reaction under consideration [Eq. (2)] proceeds at temperatures that are within the optimal range for typical concentrations.

Equation (12) denotes the maximum achievable efficiency for an ideal solar chemical process that absorbs heat from a high-temperature thermal reservoir at T_H, and rejects heat to a low-temperature thermal reservoir at T_L. Equation (15) serves to guide our choice for the cavity temperature. It presumed that $T_H = T_{cav}$. However, the actual source temperature for a solar process is the surface temperature of the sun. From this point forward, we fix $T_H = 5800\,K$ because this will provide a standard baseline for comparing the performance of different solar processes. The surroundings act as the low-temperature thermal reservoir at 298 K. Thus, our solar reactor operates between temperatures that are significantly different from those of the hot and cold thermal reservoirs. Such temperature gradients introduce irreversibilities and, consequently, reduce the system's overall efficiency. The result is that $\eta_{overall} < \eta_{overall,\,ideal} < \eta_{Carnot}$. The proceeding section presents a theoretical analysis used to evaluate $\eta_{overall}$ for the ZnO-CH_4 solar process.

4. MODELLING THE PROCESS FLOW

The process flow sheet is shown in Fig. 1. It is an archetypal model which uses a solar reactor, a heat exchanger, a quenching device, a fuel cell, a water-splitter reactor, and a heat engine. An equimolar mixture of ZnO(s) and CH_4(g) is fed into the process at $T_1 = 298K$ and pressure p. The complete process is carried out at constant pressure. In practice, pressure drops will occur throughout the system. If one assumes, however, frictionless operating conditions, no pumping work is required.

Heat Exchanger – The reactants are pre-heated in an adiabatic heat exchanger where some portion of the sensible and latent heat of the products is transferred to the reactants. The reactants enter at T_1 and exit at T_2, while the products enter at T_3 and exit at T_4. The reactants undergo a change in their equilibrium composition as they are heated, but, except for phase changes, the products are assumed to have a frozen composition as they are cooled. Two heat exchanger configurations are considered: parallel flow and counter-current flow. The pinch points† of both configurations are determined. If Q_{ex} is the total amount of power transferred from the products to the reactants and η_{ex} the heat recovery factor, then

$$Q_{ex} = \Delta H|_{Reactants\,@\,T_1,\,p \rightarrow Reactants\,@\,T_2,\,p} = -\Delta H|_{Products\,@\,T_3,\,p \rightarrow Products\,@\,T_4,\,p} \quad , \tag{16}$$

$$\eta_{ex} = Q_{ex}\Big/\left(\Delta H|_{\text{Reactants}\,@\,T_1,\,p \rightarrow \text{Products}\,@\,T_1,\,p}\right) \quad . \tag{17}$$

The chemical transformations and heat transfer across finite temperature differences during pre-heating produce the following irreversibilities that are intrinsic to the heat exchanger:

$$Irr_{ex} = \Delta S|_{Reactants\,@\,T_1,\,p \rightarrow Reactants\,@\,T_2,\,p} + \Delta S|_{Products\,@\,T_3,\,p \rightarrow Products\,@\,T_4,\,p} \quad . \tag{18}$$

A process without a heat exchanger will be also considered.

† These are the limiting points where the temperature of the heating reactants equals the temperature of the cooling products.

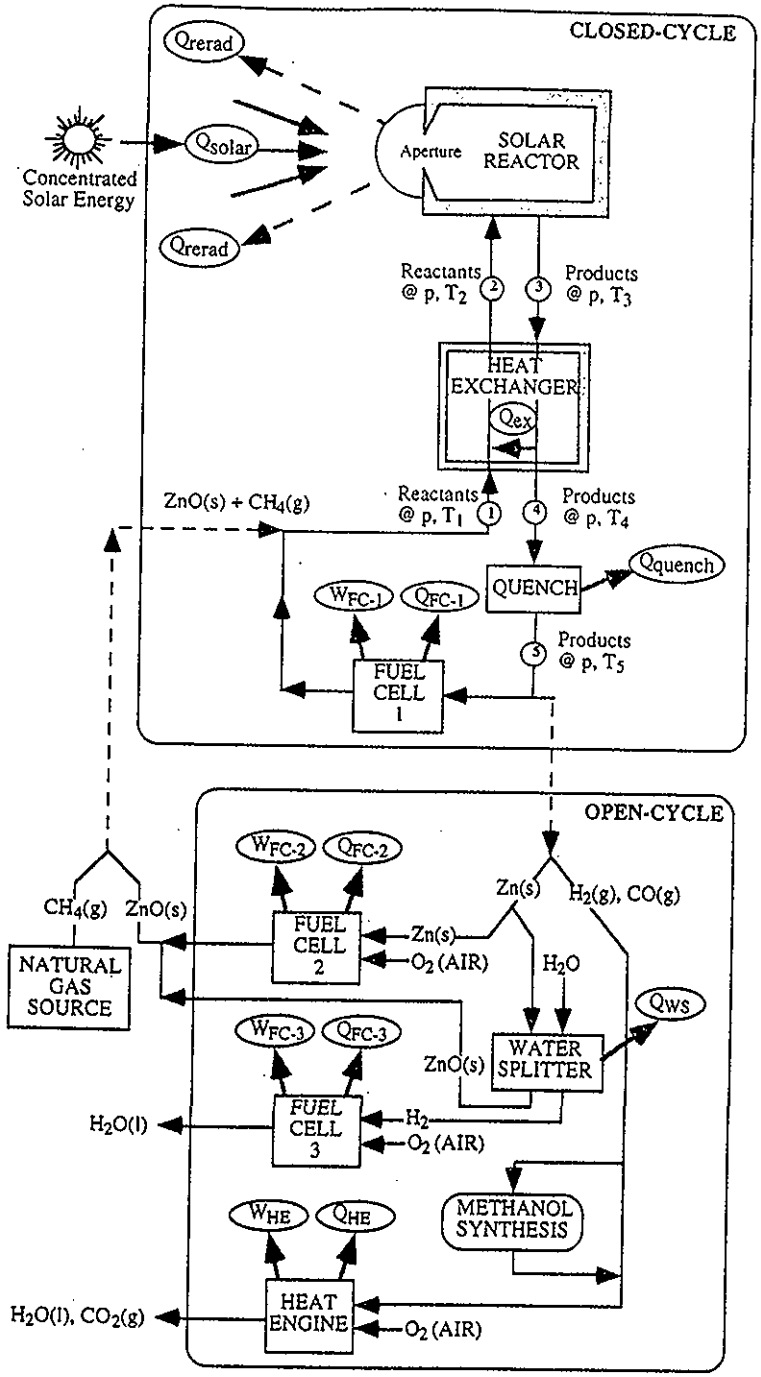

Fig. 1. The process flow diagram modelling a closed-cycle scheme that recycles all materials and an open-cycle scheme that allows for material flow into and out of the system.

Solar Reactor – After being pre-heated, the reactants enter the solar reactor at T_2 and are further heated to the cavity temperature T_{cav}. Chemical equilibrium is assumed inside the reactor. Thus, the reactants undergo a chemical transformation as they are heated to T_{cav}. Q_{solar} is the total power coming from the solar concentrator, as given by Eq. 7. The solar reactor is considered to be a perfectly insulated blackbody cavity-receiver; only radiation losses through the aperture are considered. Q_{rerad} is the power

lost by radiation as given by Eq. 5. Radiation gain from the environment is ignored. The net power absorbed in the solar reactor should match the enthalpy change of the reaction, i.e.,

$$Q_{reactor,net} = \Delta H|_{Reactants\ @\ T_2,\ p\ \rightarrow\ Products\ @\ T_3,\ p} \quad (19)$$

If I, η_{coll}, C, T_2, T_3, p, and the mass-flow rate are specified, Eq. (19) together with Eqs. (4-10) establish the required collector surface A_{coll} for delivering Q_{solar} to the solar reactor. The irreversibility in the solar reactor arises from the chemical transformation and heat transfer from the sun at 5800 K to the receiver and from the receiver to the surroundings at 298 K. Thus,

$$Irr_{reactor} = -(Q_{solar}/5800) + (Q_{rerad}/298) + \left(\Delta S|_{\text{Reactants @ } T_2,\ p\ \rightarrow\ \text{Products @ } T_3,\ p}\right) \quad (20)$$

Products exit the solar reactor at $T_3 = T_{cav}$. They have an equilibrium composition which will remain unchanged as they are cooled to T_4 in the heat exchanger, except for the phase changes. This assumption is reasonable provided zinc vapor does not catalyze the kinetics of the reverse methanation reaction. Sensible and latent heat released by the products stream are transferred to the reactants stream [see Eq. (16)].

Quench – After leaving the heat exchanger, the products are cooled rapidly to ambient temperature, $T_5 = 298K$. The amount of power lost during quenching is

$$Q_{quench} = -\Delta H|_{\text{Products @ } T_4,\ p\ \rightarrow\ \text{Products @ } T_5,\ p} \quad (21)$$

The irreversibility associated with quenching is

$$Irr_{quench} = \left(Q_{quench}/298\right) + \left(\Delta S|_{\text{Products @ } T_4,\ p\ \rightarrow\ \text{Products @ } T_5,\ p}\right) \quad (22)$$

Quenching is a completely irreversible step causing a significant drop in the system efficiency.

Closed-Cycle Scheme

Fuel Cell – From point 1 to 5 in the flow sheet, the chemical transformation

$$Reactants\ @\ 298K, p\ \rightarrow\ Products\ @\ 298K, p \quad (23)$$

has been effected. At point 5, we could calculate the overall system efficiency by introducing a reversible fuel cell, represented in Fig. 1 as FUEL CELL #1. In this ideal cell, the products recombine to form the reactants and thereby generate electrical power in an amount W_{FC-1}. Such a fuel cell does not exist and is not likely to become a reality for many years if ever; it is used here only as an intellectual concept for assigning a work value to the reaction products. It allows one to calculate the theoretical maximum available work that could be extracted from the chemical products during recombination. The work of the fuel cell is given by

$$W_{FC-1} = -\Delta G|_{Products\ @298K,\ p\ \rightarrow\ Reactants\ @298,\ p} \quad (24)$$

The fuel cell operates isothermally; Q_{FC-1} is the amount of heat rejected to the surroundings:

$$\begin{aligned} Q_{FC-1} &= -298\,K \times \Delta S|_{\text{Products @298}K,\ p\ \rightarrow\ \text{Reactants @298,}\ p} \\ &= -(\Delta H - \Delta G)|_{\text{Products @298}K,\ p\ \rightarrow\ \text{Reactants @298,}\ p}. \end{aligned} \quad (25)$$

The overall system efficiency of the closed-cycle is then calculated as

$$\eta_{overall\ CLOSED-CYCLE} = W_{FC-1}/Q_{solar} \quad (26)$$

Equation (26) allows one to evaluate complex solar thermochemical processes by considering the maximum thermodynamic value of the chemical products as they recombined to form the reactants via an ideal reversible fuel cell. The calculation makes it possible to isolate the solar process and analyze it as a closed cyclic system: a heat engine.[32] This heat engine, shown schematically in Fig. 2, uses reactants and products as the *working fluid*, exchanges heat with the surroundings, and converts solar process heat into work. This analysis provides an especially useful basis for comparing the efficiencies of different solar processes.

Check – The thermodynamic analysis is verified by performing an energy balance and by evaluating the maximum achievable efficiency (Carnot efficiency) from the total available work and from the total power input. The energy balance confirms that

$$W_{FC-1} = Q_{solar} - (Q_{rerad} + Q_{quench} + Q_{FC-1}) \quad (27)$$

The available work is calculated as the sum of the fuel-cell work plus the lost work due to irreversibilities in the solar reactor, the heat exchanger and quenching. Thus,

$$\eta_{max} = \frac{\sum Work + T_L \times \sum Irr}{Q_{input}} = \frac{W_{FC-1} + 298 \times \left(Irr_{ex} + Irr_{reactor} + Irr_{quench}\right)}{Q_{solar}} \quad (28)$$

This maximum efficiency must be equal to that of a Carnot heat engine operating between T_H and T_L, i.e.

$$\eta_{max} = \eta_{Carnot} = 1 - (T_L/T_H) = 1 - (298/5800) = 0.949 \quad (29)$$

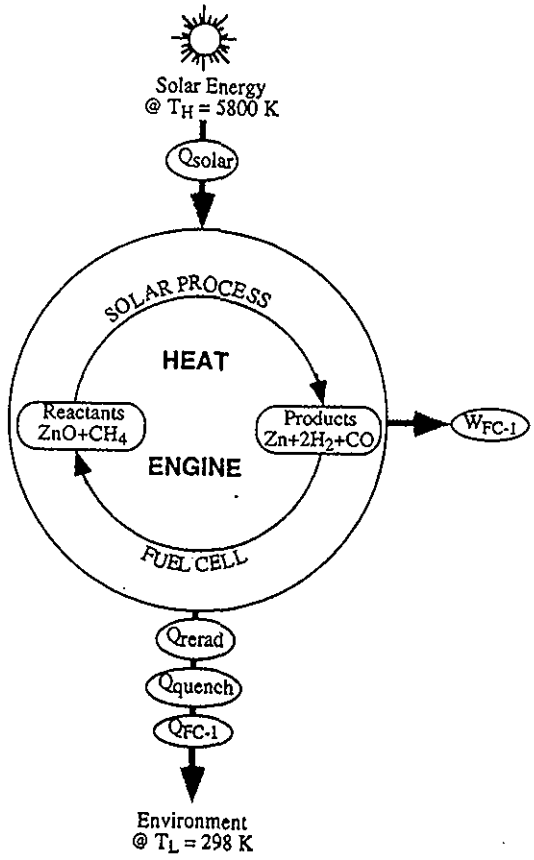

Fig. 2. The closed-cycle scheme represented as a heat engine.

Open-Cycle Scheme

Syngas as Fuel – A fuel cell that receives zinc and syngas and produces zinc oxide and methane does not exist. Thus, a pragmatic process using current technologies to extract work from the chemical products is presented in the lower box of Fig. 1. The products after quenching (point 5 in the diagram) separate naturally into Zn(s) and synthesis gas. Therefore, the separation is accomplished without expending work. Syngas, a mixture of primarily H_2 and CO, is widely utilized as a feedstock in the chemical industry for the production of synthetic fuels and commodity organic chemicals, as well as a reducing agent in the metallurgical industry (Mydrex, HYL, Armco, Purofer, Fior).[33] The syngas mixture obtained in our process has approximately a 2:1 H_2:CO molar ratio which makes it particularly suitable for methanol production. Thus, we have chosen to use syngas (or eventually methanol) as a fuel. Its combustion releases heat that is converted to work in our model via a heat engine with an efficiency of $\eta_{heat\ engine} = 35\%$, which is consistent with the value obtained in conventional power plants. The work output of the heat engine and the heat rejected to the surroundings are, respectively,

$$W_{HE} = \eta_{heat\ engine} \times \left[\Delta H|_{2H_2+CO+1.5O_2} \xrightarrow{combustion} 2H_2O(l)+CO_2\right], \quad (30)$$

$$Q_{HE} = \left(1 - \eta_{heat\ engine}\right) \times \left[\Delta H|_{2H_2+CO+1.5O_2} \xrightarrow{combustion} 2H_2O(l)+CO_2\right]. \quad (31)$$

Zinc as Fuel – Metallic zinc, the other important reaction product, is currently used primarily as a raw material in the galvanizing industry. However, zinc exhibits various intriguing advantages when considered, not as a chemical commodity, but rather as a solid fuel. Its specific calorific value is 5320 kJ/kg. It can be safely handled in air and may be easily transported. The amount of work that can be extracted from zinc depends upon how it is used. The combustion of zinc in air releases 348 kJ/mol of heat, a portion of which may be converted to work by means of a heat engine, but the efficiency of such conversion is limited by the Carnot efficiency. More efficient conversion is possible using a commercially available Zn-air battery, or a Zn-air fuel cell which is under development.[34] We have chosen to use a Zn-air fuel cell, shown in Fig. 1 as FUEL CELL #2, since it is not limited by the Carnot efficiency. Within the cell, Zn and O_2 (from air) combine electrolytically to form ZnO(s). The process generates W_{FC-2} of work while rejecting Q_{FC-2} of heat to the surroundings

$$W_{FC-2} = -\Delta G|_{Zn(s)+0.5O_2 \rightarrow ZnO(s)} \quad , \tag{32}$$

$$Q_{FC-2} = -298\,K \cdot \Delta S|_{Zn(s)+0.5O_2 \rightarrow ZnO(s)} \quad . \tag{33}$$

H_2 as Fuel – Alternatively, Zn can react with water to form molecular H_2, according to

$$Zn(s) + H_2O \xrightarrow{water-splitting} ZnO(s) + H_2 \quad . \tag{34}$$

Equation (34) takes place in the WATER-SPLITTER reactor of Fig. 1. Preliminary experimental studies have shown that this reaction proceeds at about 700 K and is exothermic. The heat liberated could be used in an auto-thermal reactor for conducting the water-splitting reaction at temperatures above ambient conditions. In this study, however, we consider this heat lost to the surroundings, as given by

$$Q_{WS} = -\Delta H|_{Zn(s)\,+\,H_2O(l) \rightarrow\, ZnO(s)\,+\,H_2} \quad . \tag{35}$$

The hydrogen produced in the water-splitter reactor may be used to enrich and adjust the syngas mixture obtained in the solar process; it may be burned in air and the heat of combustion converted into work via a heat engine, or it may be used more efficiently in a fuel cell to generate work directly. Such a cell is represented by FUEL CELL #3 in Fig. 1. W_{FC-3} is the work output and Q_{FC-3} is the heat rejected to the surroundings. The governing relations are

$$W_{FC-3} = -\Delta G|_{H_2+0.5O_2 \rightarrow H_2O(l)} \quad , \tag{36}$$

$$Q_{FC-3} = -298\,K \times \Delta S|_{H_2+0.5O_2 \rightarrow H_2O(l)} \quad . \tag{37}$$

The overall system efficiency of the open-scheme process is the ratio of work output to heat input. The work output is either $W_{HE} + W_{FC-2}$ or $W_{HE} + W_{FC-3}$, depending whether Zn is used directly in a fuel cell or to split water. The heat input is Q_{solar} plus the equivalent HHV (High Heating Value) of the methane introduced in the system. Thus,

$$\eta_{overall\,OPEN-CYCLE} = \begin{cases} (W_{HE} + W_{FC-2})/Q_{input} & \text{for a } Zn/O_2 \text{ fuel cell,} \\ (W_{HE} + W_{FC-3})/Q_{input} & \text{for an } H_2/O_2 \text{ fuel cell,} \end{cases} \tag{38}$$

where

$$Q_{input} = Q_{solar} + \left(\Delta H\Big|_{CH_4+2O_2 \xrightarrow{Combustion} CO_2+2H_2O(l)} \right) \quad . \tag{39}$$

5. RESULTS AND DISCUSSION

The baseline case is conducted at a constant total pressure of 1 atm. Calculations are also carried out for higher, industrially-preferred, pressures of 3, 5, and 10 atm. The baseline cavity temperature is taken arbitrarily equal to a value for which the chemical equilibrium mole fraction of ZnO(s) at 1 atm is less than 10^{-5}, $\therefore T_{cav} = 1250\,K$. Table 1 shows the chemical equilibrium composition of the products at the exit of the solar reactor $(T_3 = T_{cav})$, at $T_3 = 1250K$ and $p = 1$, 3, 5, and 10 atm, and at $T_3 = 1350K$ and $p = 10$ atm. Calculations were performed using the STANJAN computer code,[35] and verified using the CET-85 NASA computer code.[36] Species with mole fractions less than 10^{-5} have been omitted.

At 1 atm and at $T_{cav} \geq 1250\,K$, the reaction is nearly complete. At higher pressures, the thermodynamic equilibrium of Eq. (2) shifts to the left, as predicted by Le Chatelier's principle. For example, at 10 atm, the equilibrium composition is shifted such that the reduction of ZnO to Zn only goes to completion at or above 1350 K. Also, at 10 atm and at 1250K, condensed Zn(l) exists in equilibrium with Zn(g), but it becomes gaseous when the temperature is increased to 1350 K. The H_2:CO molar ratio is slightly altered by the pressure; it is 1.99 at 1 atm and 3 atm, and 1.98 at higher pressures. A more complete study of the ZnO + CH_4 system at 1 atm and over a wide temperature range can be found in ref. 21.

Table 1. Chemical equilibrium composition of the products at the exit of the solar reactor, calculated using STANJAN computer code and verified using the CET-85 NASA computer code.[35,36] Species with mole fractions less than 10^{-5} have been omitted.

Species and Conversion	$T_3 = 1250$ K				$T_3 = 1350$ K
	p = 1 atm	p = 3 atm	p = 5 atm	p = 10 atm	p = 10 atm
CH_4	0.01025	0.02947	0.04715	0.19255	0.04139
ZnO(s)	$< 10^{-5}$	$< 10^{-5}$	$< 10^{-5}$	0.15775	$< 10^{-5}$
Zn(g)	0.99999	0.99999	0.99999	0.63007	0.99999
Zn(l)	$< 10^{-5}$	$< 10^{-5}$	$< 10^{-5}$	0.21218	$< 10^{-5}$
H_2	1.97174	1.91880	1.87010	1.58861	1.88433
CO	0.98724	0.96333	0.94130	0.79893	0.95009
H_2O(g)	0.00775	0.02226	0.03559	0.02628	0.00329
CO_2	0.00250	0.00720	0.01154	0.00851	0.00852
H_2/CO	1.99722	1.99184	1.98671	1.98842	1.98332
CH_4-conversion	98.9%	97.1%	95.3%	80.7%	95.9%
ZnO-conversion	99.9%	99.9%	99.9%	84.2%	99.9%

Other baseline conditions include a mean flux concentration ratio of $\tilde{C} = 2000$, an optical collector efficiency of $\eta_{coll} = 100\%$, and a typical insolation of $I = 900$ W/m^2. A concentration ratio of 2000 is within the reach of large-scale solar collection facilities, such as central receivers.[37] Calculations were also carried out for $\tilde{C} = 4000$ and 8000 which can be achieved in parabolic tracking dishes or by using non-imaging secondary concentrators. The baseline mass flow rate is 1 mole/sec of Zn(s) and 1 mole/sec of CH_4 at point 1 of the process flow sheet. Unless otherwise stated, the baseline parameters are used.

Closed-cycle scheme without heat exchanger

Table 2 shows the energy balance for a closed-cycle without a heat exchanger, i.e. $T_1 = T_2$ and $T_3 = T_4$. As the operating pressure is increased at constant reactor temperature, $Q_{reactor,net}$ decreases because the enthalpy change between products and reactants is smaller: as the pressure increases, the chemical conversion decreases. $Q_{reactor,net}$ drops by 17% as the pressure is doubled from 5 to 10 atm. A_{coll} and Q_{solar} also drop by 17%. The same applies to Q_{rerad} because $\tilde{C}$ and T_{cav} are kept constant while the reactor aperture becomes smaller [see Eq. (9)], and consequently the re-radiation losses become smaller. Although $Q_{reactor,net}$ and Q_{solar} vary substantially with the operating pressure, their ratio, i.e. the solar energy absorption efficiency $\eta_{absorption}$, remains constant with pressure, as expected from Eq. (10). But $\eta_{absorption}$ decreases considerably with temperature. When the reactor temperature is raised by 100 K, $\eta_{absorption}$ drops by 3% as a result of the larger re-radiation losses. A simple expression for the direct calculation of the change in $\eta_{absorption}$ as a function of the change in temperature ΔT is given by

$$\left(1-\eta_{absorption\,@\,T}\right)\Big/\left(1-\eta_{absorption\,@\,T+\Delta T}\right)=\left[T/(T+\Delta T)\right]^4 \quad . \tag{40}$$

The overall system efficiency lies at a level of 39%. It is weakly influenced by the operating pressure, increasing monotonically with pressure in spite of the unfavourable chemical conversion. However, it drops when the temperature is increased from 1250 K to 1350 K. The energy balance and species composition for the closed-cycle scheme are presented schematically in Fig. 3 for the baseline case.

The irreversibilities in the reactor and during the quench reduce the efficiency from the Carnot value. They are produced by heat transfer across a finite temperature difference. Specifically, the reactor at 1250 or 1350 K receives radiant energy from a heat source at 5800 K and rejects a portion of it to a heat sink at 298 K. During the quench, heat transfer takes place between the hot products leaving the reactor and the cold sink. Table 2 shows that the reactor produces slightly more irreversibility than the quench. Although one can reduce the reactor irreversibility by increasing the concentration ratio (increasing $\tilde{C}$ improves $\eta_{absorption}$ by reducing the portion of incoming radiation that is reradiated to the sink) the primary irreversibility is associated with the heat transfer to the reactor across the temperature difference between T_H and T_{cav}. One may, however, be able to reduce the irreversibility of the quench. For example, if the kinetics permit the products to be cooled with a heat exchanger, one could preheat the reactants going into the solar receiver. Preheating would also reduce the irreversibility in the solar reactor, because less energy would be transferred across the large ΔT between the heat source and the reactor. We thus considered processes that included either a parallel or counter-flow heat exchanger.

Table 2. Energy balance on the closed-cycle scheme without a heat exchanger. The baseline configuration is used: $\tilde{C} = 2000$, $I = 900\,W/m^2$, $\alpha_{eff} = \varepsilon_{eff} = 1$.

	ENERGY BALANCE WITHOUT HEAT EXCHANGER $T_1 = T_2 = 298\,K$, $T_3 = T_4$				
	T_3 = 1250 K				T_3 = 1350 K
	p = 1 atm	p = 3 atm	p = 5 atm	p = 10 atm	p = 10 atm
$Q_{solar}\,[kW]$	595	590	586	486	619
$Q_{rerad}\,[kW]$	46	45	45	37	65
$Q_{reactor,net}\,[kW]$	549	545	541	449	554
$Q_{quench}\,[kW]$	237	237	238	192	249
$Q_{FC-1}\,[kW]$	84	78	74	62	72
$Irr_{reactor}/Q_{solar}\,[K^{-1}]$	10.6×10^{-4}	10.2×10^{-4}	9.9×10^{-4}	10.0×10^{-4}	10.3×10^{-4}
$Irr_{quench}/Q_{solar}\,[K^{-1}]$	8.3×10^{-4}	8.6×10^{-4}	8.7×10^{-4}	8.3×10^{-4}	8.8×10^{-4}
$W_{FC-1}\,[kW]$	228	230	229	195	233
$\eta_{absorption}\,[\%]$	92.3				89.5
$\eta_{Carnot}\,[\%]$	94.9				94.9
$\eta_{overall,ideal}\,[\%]$	87.6				84.9
$\eta_{overall}\,[\%]$	38.6	38.9	39.1	40.2	37.8

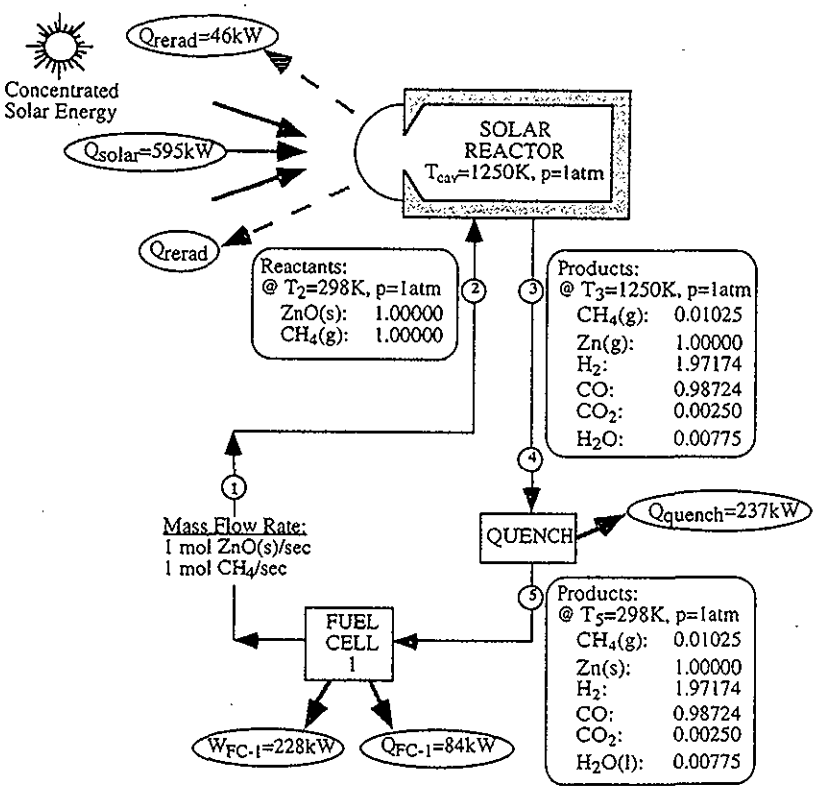

Fig. 3. Energy balance of the closed-cycle scheme without an heat exchanger. The following baseline parameters are used: $\tilde{C} = 2000$, $I = 900\,W/m^2$, $\alpha_{eff} = \varepsilon_{eff} = 1$, $T_3 = 1250\,K$, $p = 1\,atm$.

Closed-cycle scheme with parallel-flow heat exchanger

Table 3 shows the energy balance calculation of the closed-cycle scheme when a parallel-flow heat exchanger is included, i.e. $T_1 = 298\,K < T_2$, $T_3 = 1250\,K > T_4$, and, at the limit, $T_2 = T_4$. The results are also presented schematically in Fig. 4 for the baseline case. Note that the composition of the reactants varies through the heat exchanger as they are heated from point 1 at $T_1 = 298$ K to point 2 at $T_2 = 940$ K. Carbon is found in the equilibrium composition. Although carbon deposition is thermodynamically favorable at temperatures below 1200 K, it is unlikely that it ever reaches a state of equilibrium because the kinetics of carburization are usually slow and require the nucleation of carbon on some catalytic site. The presence of freshly formed zinc might under certain conditions weakly catalyze the CH_4-cracking reaction.[21] The composition of the products remains constant as they are cooled in the heat exchanger, except for the Zn(g) and H_2O(g) that undergo condensation.

Table 3. Energy balance on the closed-cycle scheme with a heat exchanger. The baseline configuration is used: $C = 2000$, $I = 900\,W/m^2$, $\alpha_{eff} = \varepsilon_{eff} = 1$, $T_3 = 1250\,K$, $p = 1\,atm$.

	ENERGY BALANCE WITH HEAT EXCHANGER $T_1 = 298\,K < T_2$, $T_3 = 1250\,K > T_4$	
	Parallel Flow $T_2 = T_4 = 940\,K$	**Counter-current Flow** $T_2 = 1066\,K$, $T_4 = 400\,K$
$Q_{solar}\,[kW]$	448	351
$Q_{rerad}\,[kW]$	34	27
$Q_{reactor,\,net}\,[kW]$	414	324
$Q_{ex}\,[kW]$	135	225
$Q_{quench}\,[kW]$	102	12
$Q_{FC-1}\,[kW]$	84	
$Irr_{reactor}/Q_{solar}\,[K^{-1}]$	9.31×10^{-4}	9.13×10^{-4}
$Irr_{ex}/Q_{solar}\,[K^{-1}]$	1.58×10^{-4}	0.76×10^{-4}
$Irr_{quench}/Q_{solar}\,[K^{-1}]$	3.90×10^{-4}	0.14×10^{-4}
$W_{FC-1}\,[kW]$	228	
$\eta_{absorption}\,[\%]$	92.3	
$\eta_{Carnot}\,[\%]$	94.9	
$\eta_{overall,\,ideal}\,[\%]$	87.6	
$\eta_{ex}\,[\%]$	56.9	94.9
$\eta_{overall}\,[\%]$	50.8	64.9

The temperature at point 2 is found by plotting $\Delta H = f(T)$ for the reactants and products streams and arranging both curves as shown in Fig. 5a. The slope of these curves is $C_{p,\,mixture}$, the specific heat capacity of the mixture. $C_{p,\,mixture}$ varies with temperature because the mixture composition, the components' phases, and the C_p of the individual species vary with temperature. ΔH of the reactants varies monotonically with temperature, with a significant gradient in the 1000-1150K range where most of the reaction occurs. Similarly, the ΔH of the products exhibits a noticeable gradient in the neighbourhood of the zinc boiling point (1180 K) due to the heat of vaporization, and a discontinuity at the zinc melting point (692 K) due to the heat of fusion. The intersection of these two curves determines the temperature at the "pinch-point": $T_2 = 940\,K$. Heating the reactants beyond $940K$ is not possible because heat cannot flow spontaneously from the colder products to the hotter reactants. The total heat transferred is $135kW$. This recovery amounts to 57% of the sensible and latent heat available in the products. The remainder of the energy is rejected to the surroundings by the quenching. As expected, Table 3 indicates that the irreversibilities per Q_{solar} in the reactor and during cooling are reduced by means of the heat exchanger. These improvements increase the process efficiency by 12%.

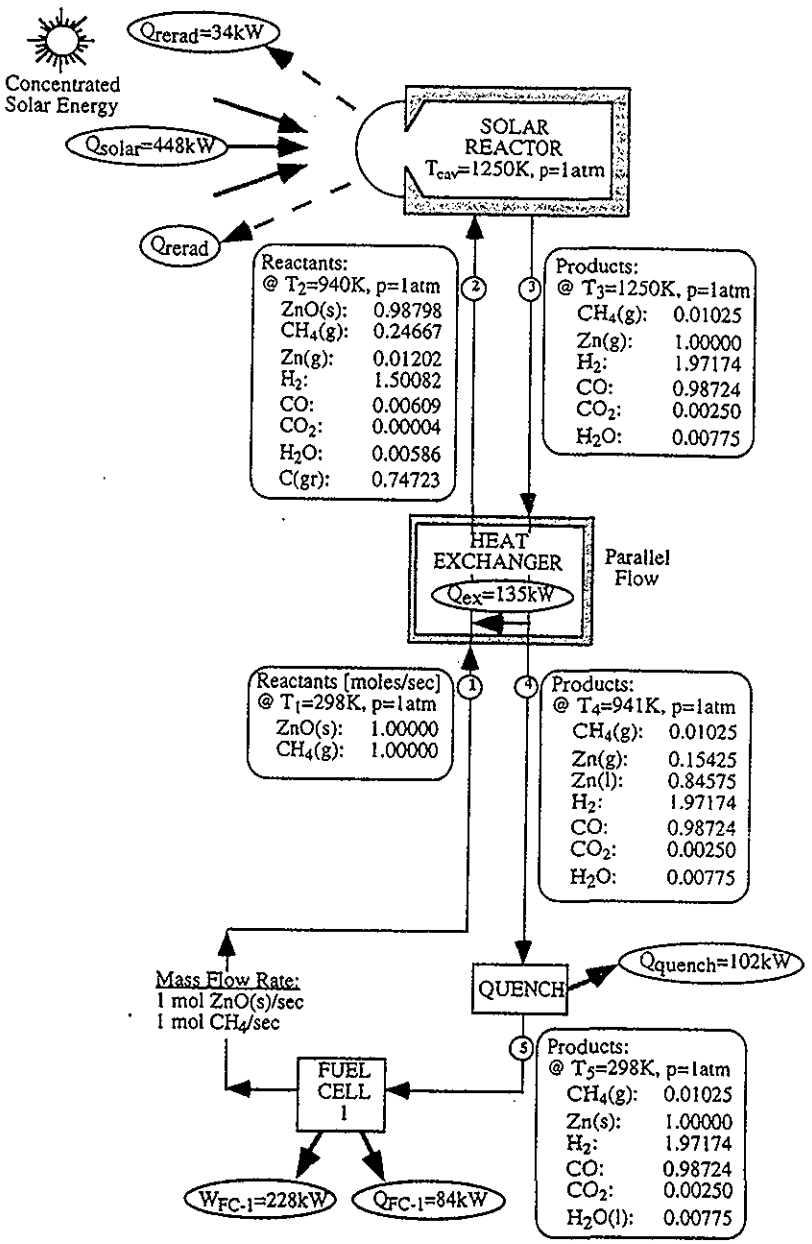

Fig. 4. Energy balance of the closed-cycle scheme when a parallel-flow heat exchanger is employed. The baseline parameters are used.

Closed-cycle scheme with counter-current-flow heat exchanger

Table 3 also shows the energy balance calculation when a counter-current-flow heat exchanger is included, i.e. $T_1 = 298\,K < T_2$, $T_3 = 1250\,K > T_4$, and, at the limit, $T_1 = T_4$. Analogous to the parallel-flow, the exit temperatures are found by plotting $\Delta H = f(T)$ for the reactants and products streams and arranging both curves as shown in Fig. 5b. A pinch point forces the products exit temperature to be no less than 400 K. The exit temperature of the reactants stream is found graphically in Fig. 5b or analytically by solving Eq. 16. It yields $T_3 = 1066\,K$. Most of the sensible and latent heat available in the hot products, about $225\,kW$, could in principle be transferred to pre-heat the reactants. The heat recovery

factor reaches 95%. In practice, such high recovery efficiency cannot be achieved because of the finite dimensions of the heat exchanger and because the rate of heat transfer approaches zero when ΔT across the counter-current flows is small. None-the-less, the counter-current-flow heat exchanger offers a significantly higher heat recovery factor than that attained for the parallel-flow heat exchanger. The overall cycle efficiency is 65%, which is 14% higher than the efficiency obtained for the parallel-flow heat exchanger and 26% higher than that obtained without a heat exchanger. The energy balance and species composition for a closed-cycle scheme with a counter-current-flow heat exchanger are presented schematically in Fig. 6.

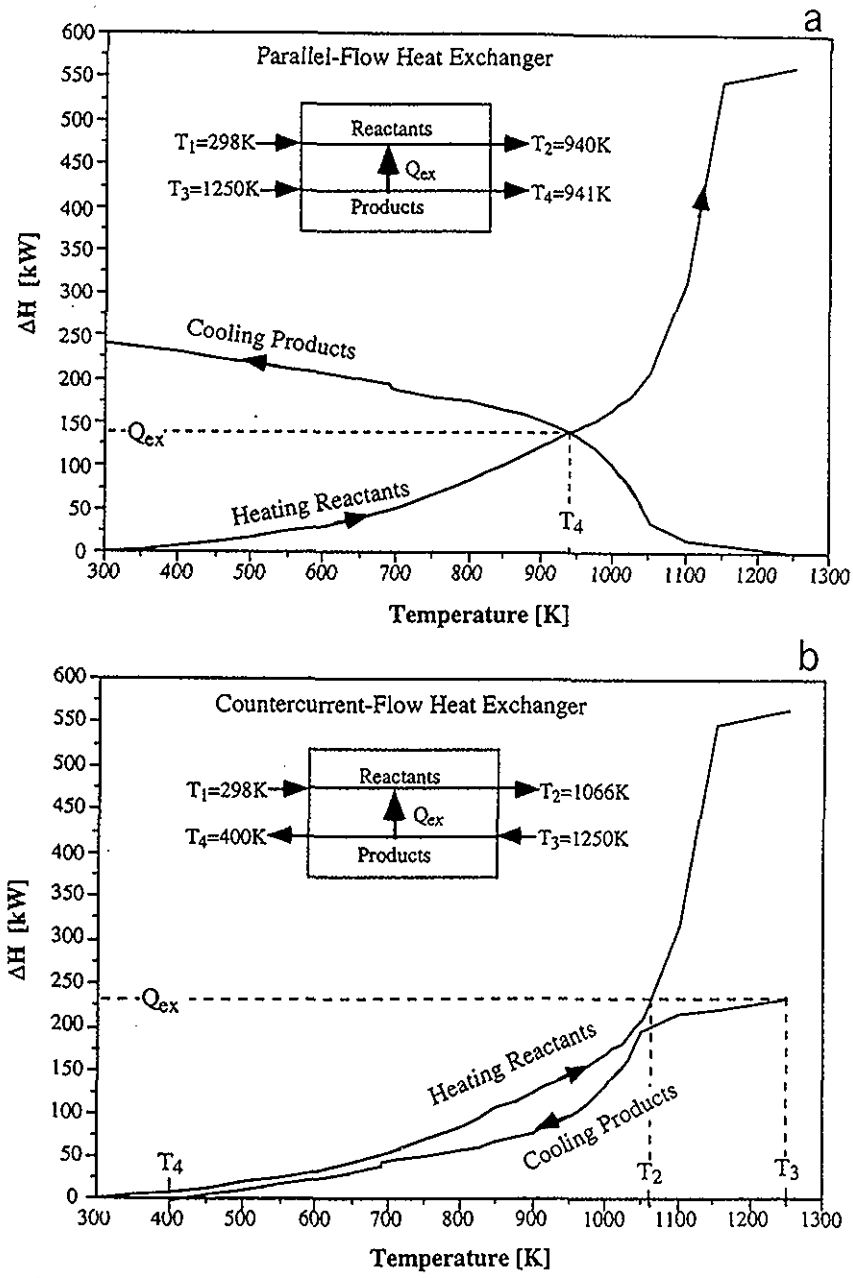

Fig. 5. Enthalpy change as a function of temperature for the reactants and products. The reactants undergo a change in their chemical equilibrium composition as they are heated. The composition of the products remains constant as they are cooled, except for phase changes. The inlet and outlet temperatures and the heat transferred are shown in Fig. 5a for the parallel-flow heat exchanger and in Fig. 5b for the counter-current-flow heat exchanger.

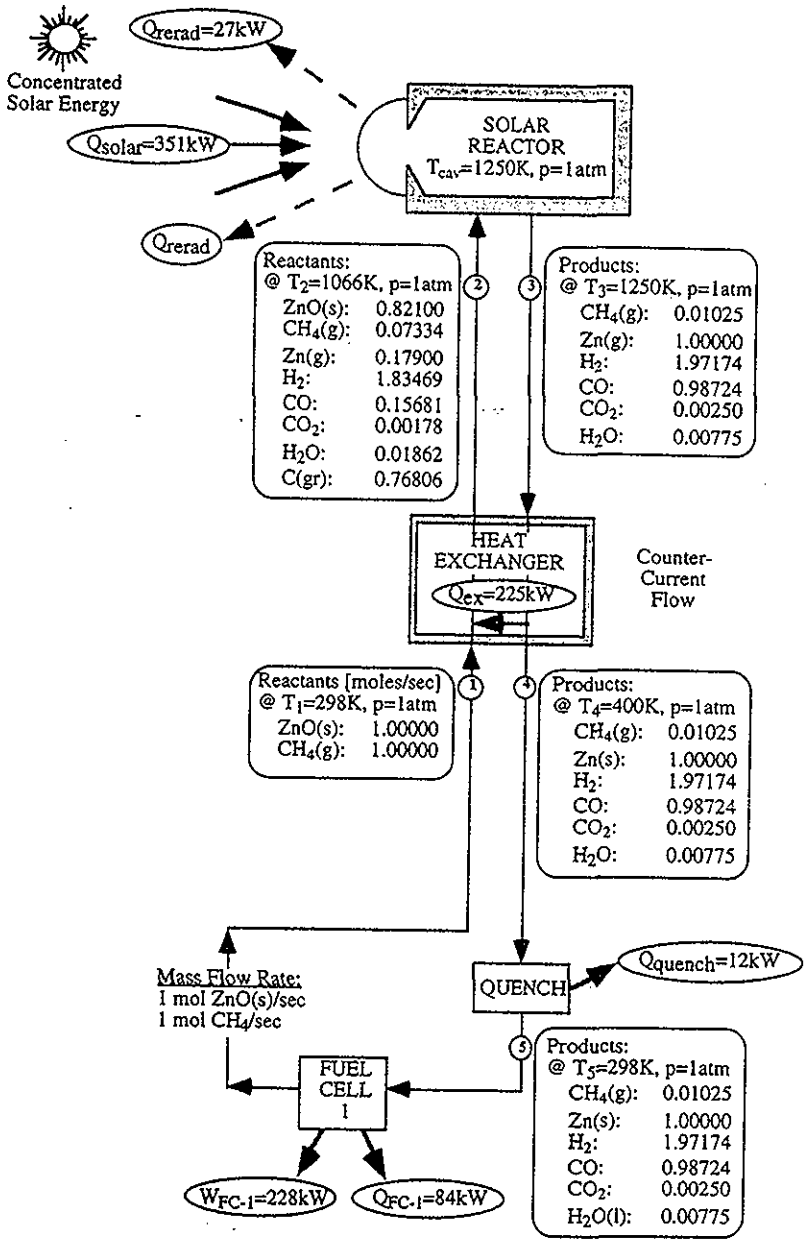

Fig. 6. Energy balance of the closed-cycle process when a counter-current flow heat exchanger is employed. The baseline parameters are used.

The effect of the solar concentration on the overall efficiency is shown in Fig. 7, for the closed-cycle scheme with and without heat exchanger. Obviously, the higher the concentration, the smaller the aperture, the less re-radiation losses, and consequently the higher the overall efficiency. However, the cycle efficiency is a weak function of $\tilde{C}$ and doubling or even quadrupling the concentration brings about just a small improvement in the overall efficiency.

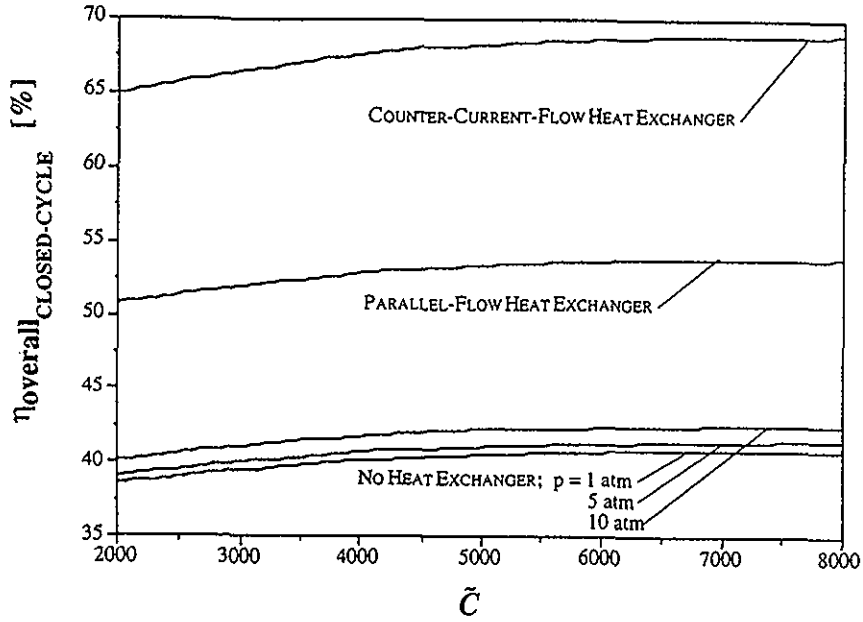

Fig. 7. Variation of the overall efficiency with solar concentration, for the closed-cycle scheme with and without heat exchanger. The baseline parameters are used. The overall efficiency increases dramatically as a portion of the available sensible heat is recovered, but increasing concentration ratios produce only small improvements in the cycle efficiency.

Open-cycle scheme

Finally, the open-cycle scheme is analyzed for the baseline case, with and without a heat exchanger. Notice that the chemical products at point 5 in Fig. 1 do not have the exact stoichiometric composition given by Eq. (2) due to the incomplete CH_4 conversion. (The equilibrium composition at point 5 was given in Figs. 3, 4 or 6). At this point the products undergo natural phase separation into solid zinc and gas phases. The syngas mixture (having a H_2:CO molar ratio of 1.94) is combusted in the heat engine. Zinc is sent either to the Zn/O_2 fuel cell or to the water-splitter reactor for H_2 production.

Table 4 shows the complete energy balance of the open-cycle scheme. Evidently, $\eta_{overall}$ is higher when heat exchangers are employed because the required Q_{solar} is significantly lower. Also superior by about 13% is the efficiency of the scheme that uses Zn directly in a Zn/O_2 fuel cell, as compared to using Zn for splitting water and sending H_2 to a H_2/O_2 fuel cell. The reason is that, on a molar basis,

$$\Delta G|_{Zn(s)+0.5O_2 \rightarrow ZnO(s)} > \Delta G|_{H_2+0.5O_2 \rightarrow H_2O(l)} \,. \tag{41}$$

and the Zn/O_2 fuel cell delivers more work than the H_2/O_2 fuel cell. The difference in the work output between the two fuel cells is equal to the difference between the heat rejected plus the heat losses in the exothermic water-splitting reaction, i.e.

$$\underbrace{W_{FC-2}+Q_{FC-2}}_{\Delta H|_{Zn(s)+0.5O_2 \rightarrow ZnO(s)}} = \underbrace{W_{FC-3}+Q_{FC-3}}_{\Delta H|_{H_2+0.5O_2 \rightarrow H_2O(l)}} + \underbrace{Q_{WS}}_{\Delta H|_{Zn(s)+H_2O(l) \rightarrow ZnO(s)+H_2}} \,. \tag{42}$$

The overall efficiencies for the open-cycle schemes with and without heat exchangers are lower than the corresponding closed-cycle schemes, principally because of the losses incurred in the heat engine. The heat rejected by the heat engine amounts to 550 kW when a 35% engine efficiency is assumed.

Chemical by-products– The chemical products from each open-system component are either recycled or discarded. The products of the HEAT ENGINE are H_2O and CO_2, which are discharged to the atmosphere. The product of the FUEL CELL #2 is ZnO(s), which is recycled to the solar reactor. The products of the WATER SPLITTER are ZnO(s) and H_2; ZnO(s) is recycled to the solar reactor while H_2 is directed to the FUEL CELL #3. The product of the FUEL CELL #3 is H_2O, which is vented to the atmosphere. An external source of natural gas is required for supplying CH_4, which, together with

ZnO(s), are the feedstock into the solar reactor. The CO_2 emissions from the open-cycle scheme are only those resulting from the combustion of the syngas, expressed in units of specific CO_2 emissions per electricity generation:

$$\text{specific } CO_2 \text{ emissions for the open-cycle} = 0.26 \text{ kg } CO_2/\text{ kWh}_e \ . \tag{43}$$

For comparison, using the HHV of methane for generating electricity in a power plant with the same 35% efficiency releases 0.51 kg CO_2/KWh$_e$, i.e. twice as much CO_2 as generated by the proposed solar open-cycle process.

Table 4. Energy balance on the open-cycle scheme with and without a heat exchanger. The baseline configuration is used: $\tilde{C} = 2000$, $I = 900\,W/m^2$, $\alpha_{eff} = \varepsilon_{eff} = 1$, $T_1 = 298\,K, T_3 = 1250\,K$, $p = 1\,atm$.

	No Heat Exchanger $T_1 = T_2 = 298\,K$ $T_3 = T_4 = 1250\,K$	Parallel Flow Heat Exchanger $T_2 = T_4 = 940\,K$	Counter-current Flow Heat Exchanger $T_2 = 1066\,K$ $T_4 = 400\,K$
$Q_{solar}\,[kW]$	595	448	351
$Q_{rerad}\,[kW]$	46	34	27
$Q_{reactor,\,net}\,[kW]$	549	414	324
$Q_{ex}\,[kW]$	0	135	225
$Q_{quench}\,[kW]$	237	102	12
$Q_{FC-2}\,[kW]$	30		
$Q_{FC-3}\,[kW]$	49		
$Q_{WS}\,[kW]$	63		
$Q_{HE}\,[kW]$	554		
$W_{FC-2}\,[kW]$	318		
$W_{FC-3}\,[kW]$	236		
$W_{HE}\,[kW]$	298		
$\eta_{overall}\,[\%]$ (Zn to Fuel Cell)	41.5	46.0	49.6
$\eta_{overall}\,[\%]$ (H_2 to Fuel Cell)	36.0	39.9	43.1

CONCLUSIONS

The combined ZnO-reduction and CH_4-reforming, using solar radiation concentrated 2000 times as the energy source of process heat, could be conducted with maximum closed-cycle efficiencies between 40 and 65%, depending on the heat-recovery factor of the heat exchanger. A reactor temperature of 1250K and a pressure of 1 atm appear to be the optimum operating conditions. Higher temperatures result in higher re-radiation losses while higher pressures result in lower quality chemical products. The open-cycle scheme that extracts work from the products in technically, more readily, feasible processes features maximum overall efficiencies between 36 and 50%, depending on the heat-recovery factor and whether a Zn/O_2 or an H_2/O_2 fuel cell is employed. Major sources of irreversibilities are those associated with the re-radiation losses of the solar reactor and the heat rejected during the quenching.

The proposed thermochemical process combines fossil and solar energies. It helps create a technological link between the current fossil-fuel-based power plants and the future solar chemical plants. The second-law analysis is a useful theoretical tool for assessing maximum achievable efficiencies, for investigating the influence of the operating conditions, and for establishing a base for comparing different thermochemical processes.

Acknowledgements- This work was supported by the BEW-Swiss Federal Office of Energy and by the Paul Scherrer Institute in the form of a Visiting Scientist award to R. Palumbo during the summer of 1995.

NOMENCLATURE

$A_{aperture}$	area of reactor aperture (m^2)
$C_{p,\,mixture}$	specific heat capacity of the mixture (kJ mol^{-1} K^{-1})
$\bar{C}$	mean flux solar concentration
ΔG	Gibbs free energy change (kW)
ΔH	enthalpy change (kW)
I	normal beam insolation (kW/m^2)
Irr_{ex}	irreversibility associated with the heat exchanger (kW K^{-1})
Irr_{quench}	irreversibility associated with the quenching (kW K^{-1})
$Irr_{reactor}$	irreversibility associated with the solar reactor (kW K^{-1})
$Q_{absorbed}$	power absorbed by the solar reactor (kW)
$Q_{aperture}$	incoming solar power intercepted by the reactor aperture (kW)
Q_{FC}	heat rejected to the surroundings by the fuel cell (kW)
Q_{HE}	heat rejected to the surroundings by the heat engine (kW)
Q_{quench}	heat rejected to the surroundings by the quenching process (kW)
$Q_{reactor,\,net}$	net power absorbed by the solar reactor (kW)
Q_{rerad}	power re-radiated through the reactor aperture (kW)
Q_{solar}	total solar power coming from the concentrator (kW)
Q_{WS}	heat rejected to the surroundings by the water-splitter (kW)
ΔS	entropy change (kW)
T_{cav}	nominal cavity-receiver temperature (K)
T_L	temperature of surroundings (298 K)
T_H	sun surface temperature (5800 K)
T_{max}	maximum temperature of the solar cavity-receiver
T_{opt}	optimal temperature of the solar cavity-receiver for maximum $\eta_{overall,\,ideal}$
W_{FC}	work output by the fuel cell (kW)
W_{HE}	work output by the heat engine (kW)
α_{eff}	effective absorptance of the solar cavity-receiver
ε_{eff}	effective emittance of the solar cavity-receiver
$\eta_{absorption}$	solar energy absorption efficiency
η_{Carnot}	efficiency of a Carnot heat engine operating between T_H and T_L
η_{coll}	efficiency of the solar collection system
η_{ex}	heat recovery factor of the heat exchanger
$\eta_{heat\ engine}$	efficiency of the heat engine
$\eta_{overall}$	Overall system efficiency
$\eta_{overall,\,ideal}$	Overall efficiency of an ideal system
σ	Stefan-Boltzmann constant (5.6705×10^{-8} $Wm^{-2}K^{-4}$)

REFERENCES

1. A . Steinfeld and E. A. Fletcher, *Energy - The International Journal* 16, 1011 (1991).
2. D. A. Duncan and H. A. Dirksen, SERI/TR-98326-1, Boulder, CO (1980).
3. H. Eicher, Ph.D. Thesis, Universität Basel (1985).
4. R. D. Palumbo, M. B. Campbell, and T. H. Grafe, *Energy - The International Journal* 17, 179 (1992).
5. J. P. Murray, A. Steinfeld, and E. A. Fletcher, *Energy - The International Journal* 20, 695 (1995).
6. R. D. Palumbo, Ph.D. Thesis, University of Minnesota, Minneapolis, MN (1987).
7. R. D. Palumbo and E. A. Fletcher, *Energy - The International Journal* 13, 319 (1988).
8. A. Tofighi and F. Sibieude, *Int. J. Hydrogen Energy* 5, 375 (1980).
9. F. Sibieude, M. Ducarroir, A. Tofighi, and J. Ambriz, *Int. J. Hydrogen Energy* 7, 79 (1982).
10. A. Tofighi, Ph.D. Thesis, L'Institut National Polytechnique de Toulouse (1982).

11. P. Kuhn, K. Ehrensberger, E. Steiner, A. Steinfeld, *Solar Engineering 1995*, pp. 375-380, Hawaii (March 19-24, 1995).
12. A. Steinfeld, *C&E'95 - Proc. Int. Symp. CO_2 Fixation and Efficient Utilization of Energy*, pp. 123-132, Tokyo (Nov. 29-Dec. 1, 1993).
13. S. Huwyler and W. Seifritz, *Nature* **255**, 188 (1975).
14. D. Barret, *Ind. Eng. Chem. Process Des. Develop.* **11**, 415 (1972).
15. D. Ghosh, A. K. Roy, and A. Ghosh, *Transactions Iron Steel Inst. Jpn.* **26**, 186 (1986).
16. L. A. Haas, J. C. Nigro, and R. K. Zahl, Bureau of Mines Report RI-8997, U. S. Department of Interior (1985).
17. P. Ruprecht and M. Baerns, *Chemie-Ing. Techn.* **43**, 894 (1971).
18. K. M. Hutchings, R. J. Hawkins, and J. D. Smith, *Ironmaking and Steelmaking* **15**, 121 (1988).
19. A. Steinfeld, A. Frei, and P. Kuhn, *Metallurgical and Materials Transactions* **26B**, 509 (1995).
20. A. Steinfeld, P. Kuhn, and J. Karni, *Energy - The International Journal* **18**, 239 (1993).
21. A. Steinfeld, A. Frei, P. Kuhn, and D. Wuillemin, *Int. J. Hydrogen Energy* **20**, 793 (1995).
22. A. Steinfeld and G. Thompson, *Energy - The International Journal* **19**, 1077 (1994).
23. A. Steinfeld, P. Kuhn, and Y. Tamaura, *Energy Conversion and Management* (in press, 1995).
24. R. B. Diver, *J. Solar Energy Engineering* **109**, 199 (1987).
25. A. Steinfeld and M. Schubnell, *Solar Energy* **50**, 19, (1993).
26. E. M. Sparrow and R. D. Cess, *Radiation Heat Transfer*, Wadsworth Publishing Co., Belmont, USA (1966).
27. W. T. Welford and R. Winston, *High Collection Nonimaging Optics*, Academic Press, San Diego, USA (1989).
28. J. Ganz, P. Haueter, A. Steinfeld, and D. Wuillemin, *Proc. 7th Int. Symp. Solar Thermal Concentrating Technologies*, Vol. 4, pp. 826-832, Moscow (Sept. 26-30, 1994).
29. A. Steinfeld, A. Imhof, and D. Mischler, *J. Solar Energy Engineering* **114**, 171 (1992).
30. A. Steinfeld, A. Imhof, and E. A. Fletcher, *Proc. 6th Int. Symp. Solar Thermal Concentrating Technologies*, pp. 501-510, Mojacar, Spain (Sept. 28-Oct. 2, 1992).
31. A. Steinfeld, M. Schubnell, *Proc. 6th Int. Symp. Solar Thermal Concentrating Technologies*, pp. 491-500, Mojacar, Spain (Sept. 28-Oct. 2, 1992).
32. E. A. Fletcher, *J. Minnesota Academy of Science* **49**, 30 (1983).
33. C. G. Davis, J. F. McFarlin, and H. R. Pratt, *Ironmaking and Steelmaking* **9**, 93 (1982).
34. J. C. Salas-Morales and J. W. Evans, *J. Applied Electrochemistry* **24**, 858 (1994).
35. W. C. Reynolds, "The Element Potential Method for Chemical Equilibrium Analysis", Stanford University, Palo Alto, CA (1986).
36. S. Gordon and J. B. McBride, "Computer Program for Calculation of Complex Chemical Equilibrium Composition, Rocket Performance, Incident and Reflected Shocks, And Chapman-Jouguet Detonations", NASA SP-273, NASA Lewis Research Center, Cleveland, 1976. A PC-version devised by T. Kappauf, M. Pipho, and E. Whitby for E. A. Fletcher at the University of Minnesota was used in this study (1987).
37. C. J. Winter, R. L. Sizmann, and L. L. Vant-Hull, *Solar Power Plants*, Springer-Verlag (1991).